Generating ultradense pair beams using 400 GeV/*c* protons

C. D. Arrowsmith,[1,*] N. Shukla,[2] N. Charitonidis,[3] R. Boni,[4] H. Chen,[5] T. Davenne,[6] A. Dyson,[1] D. H. Froula,[4] J. T. Gudmundsson,[7,8] B. T. Huffman,[1] Y. Kadi,[3] B. Reville,[9] S. Richardson,[10] S. Sarkar,[1] J. L. Shaw,[4] L. O. Silva,[11] P. Simon,[3] R. M. G. M. Trines,[6] R. Bingham,[6,12] and G. Gregori[1]

[1]*Department of Physics, University of Oxford, Parks Road, Oxford OX1 3PU, United Kingdom*
[2]*CINECA High-Performance Computing Department, Via Magnanelli 6/3, 40033 Casalecchio di Reno - Bologna, Italy*
[3]*European Organization for Nuclear Research (CERN), CH-1211 Geneva 23, Switzerland*
[4]*University of Rochester Laboratory for Laser Energetics, Rochester, New York 14623, USA*
[5]*Lawrence Livermore National Laboratory, 7000 East Avenue, Livermore, California 94550, USA*
[6]*Rutherford Appleton Laboratory, Chilton, Didcot OX11 0QX, United Kingdom*
[7]*Science Institute, University of Iceland, Dunhaga 3, IS-107 Reykjavik, Iceland*
[8]*Department of Space and Plasma Physics, School of Electrical Engineering and Computer Science, KTH Royal Institute of Technology, SE-100 44 Stockholm, Sweden*
[9]*Max-Planck-Institut für Kernphysik, Saupfercheckweg 1, D-69117 Heidelberg, Germany*
[10]*Atomic Weapons Establishment, Aldermaston, Reading, Berkshire RG7 4PR, United Kingdom*
[11]*GoLP/Instituto de Plasmas e Fusão Nuclear, Instituto Superior Técnico, Universidade de Lisboa, 1049-001 Lisboa, Portugal*
[12]*Department of Physics, University of Strathclyde, Glasgow G4 0NG, United Kingdom*

(Received 16 November 2020; accepted 6 April 2021; published 10 May 2021)

An experimental scheme is presented for generating low-divergence, ultradense, relativistic, electron-positron beams using 400 GeV/*c* protons available at facilities such as HiRadMat and AWAKE at CERN. Preliminary Monte Carlo and particle-in-cell simulations demonstrate the possibility of generating beams containing 10^{13}–10^{14} electron-positron pairs at sufficiently high densities to drive collisionless beam-plasma instabilities, which are expected to play an important role in magnetic field generation and the related radiation signatures of relativistic astrophysical phenomena. The pair beams are quasineutral, with size exceeding several skin depths in all dimensions, allowing the examination of the effect of competition between transverse and longitudinal instability modes on the growth of magnetic fields. Furthermore, the presented scheme allows for the possibility of controlling the relative density of hadrons to electron-positron pairs in the beam, making it possible to explore the parameter spaces for different astrophysical environments.

DOI: 10.1103/PhysRevResearch.3.023103

I. INTRODUCTION

The environmental conditions in the magnetospheres of pulsars, magnetars, and black holes are known to present sites of copious electron-positron pair production [1–6]. Outflows from these compact objects, in the form of winds or collimated jets, are inevitably pair-plasma enriched. The energy dissipation mechanisms, which ultimately determine the electromagnetic radiative signatures we measure from Earth, are expected to differ substantially from equivalent electron-ion outflows.

A particular case of pair-dominated outflows involves those thought to generate gamma-ray bursts (GRBs) [7,8]. GRBs are among the most luminous events in the universe, yet the precise nature of the emission remains unresolved. It is commonly believed that GRBs result from synchrotron emission of relativistic particles energized at internal shocks [9,10]. In both the prompt and afterglow GRB emission, it is expected that filamentation-type kinetic beam-plasma instabilities [11–13] are responsible for the growth of magnetic fields associated with the synchrotron emission [14,15], and simulations have suggested that the required field strengths can be amplified in the kind of relativistic collisionless shocks expected to be relevant to GRBs [16,17]. Nevertheless, such studies are constrained by the ability of numerical techniques to fully capture the extreme conditions in GRB outflows. This motivates the development of experimental platforms which can complement simulation studies in exploring the nonlinear aspects of beam-plasma instabilities for a range of compositions and densities of beam and background plasmas.

In this paper, we introduce an experimental scheme for generating electron-positron beams using 400 GeV/*c* protons available at facilities such as HiRadMat [18] and AWAKE [19] at CERN. Preliminary Monte Carlo simulations which model this scheme indicate the possibility of generating low-divergence beams of 10^{13}–10^{14} electron-positron pairs with sufficiently high densities to drive filamentation-type beam-plasma instabilities on observable laboratory scales.

*charles.arrowsmith@physics.ox.ac.uk

This number of pairs is significantly higher (by several orders of magnitude) than previously reported laser-produced quasineutral pair beams [20–24].

As well as electron-positron pairs, the beams expected to be generated contain a smaller density of hadrons such as protons and pions. The scheme we introduce allows for the possibility to control the density of these particles relative to electron-positron pairs by several orders of magnitude. This is useful because jet composition remains an important unresolved question surrounding the powering of GRBs. In the fireball model of GRBs, baryon loading of the jet is discussed as an important parameter in determining the Lorentz factor of the stream [7], and the role of photoproduction of mesons (and also neutrons and neutrinos) at internal shocks of the fireball model has been discussed as an explanation for anomalous spectral components in the observed prompt emission [25,26]. The effect of streaming ions on the growth and saturation of magnetic fields via filamentation-type instabilities has been investigated in particle-in-cell (PIC) simulations [27] and can now be explored experimentally.

Furthermore, the generated beams have sufficient longitudinal extent to observe obliquely growing instability modes that are otherwise suppressed in shorter beams [23]. This is important because obliquely growing instability modes that compete with transverse current filamentation instability are expected to affect the fraction of bulk kinetic energy of the beam which is converted into magnetic and electric fields, and hence are important for modeling radiative emission processes.

This paper presents simulations and experimental feasibility of the introduced experimental setup. We show preliminary results of Monte Carlo simulations characterizing the generated electron-positron-hadron beams and present PIC simulations modeling the propagation of these beams through a background plasma in the laboratory. These simulations demonstrate the development of kinetic instabilities and the growth of feasibly measurable magnetic fields exceeding magnitudes of 0.1 T.

II. EXPERIMENTAL SCHEME

High-Radiation to Materials (HiRadMat) [18] and Advanced Proton Driven Plasma Wakefield Acceleration Experiment (AWAKE) [19] are facilities at CERN which can provide high-intensity 400 GeV/c proton beams up to a maximum intensity of several 10^{11} protons per 400-ps bunch. A summary of the beam parameters of these facilities is given in Table I.

TABLE I. Beam parameters for 400 GeV/c proton facilities HiRadMat [18] and AWAKE [19]. The p^+ bunch intensity is given in number of protons per bunch.

Parameter	HiRadMat	AWAKE
Beam momentum (GeV/c)	440	400
p^+ bunch intensity	1.2×10^{11}	3×10^{11}
Bunch duration (1σ) (ps)	375	400
Beam radius (1σ) (mm)	0.25–4	0.2

In proton-nucleon interactions with center-of-mass energy $\sqrt{s}$ in excess of GeV, particles produced in hadronic interactions come mostly from the hadronization of quarks and gluons. A shower of protons, pions, kaons, and other hadrons is observed. In particular, a significant component of this shower is a copious number of neutral pions, each of which undergoes electromagnetic decay to two photons on a timescale $\mathcal{O}(10^{-16}$ s) in the π^0 rest frame. A highly directional beam of GeV-energy photons is produced in the target, which predominantly loses energy via e^+e^- pair production. The generated e^+e^- lose energy via the generation of bremsstrahlung at a rate approximately proportional to their energy, and so a cascade of copious e^+e^- and γ develops. This represents the dominant channel for production of electron-positron pairs initiated with a GeV/c proton beam.

For ultrarelativistic streams such as the pair beam systems we generate in this scheme, and those relevant to GRBs (in which Lorentz factors are expected to be in the range $\gamma_b \sim 10^2$–10^6), transverse current filamentation instability (CFI) and oblique instability (OBI) will be the dominant beam-plasma instabilities leading to growth of magnetic fields [15]. The growth of these instabilities is observed when the physical beam size exceeds the skin depth of the background plasma (c/ω_p), where $\omega_p = \sqrt{4\pi n_e e^2/m_e}$ is the plasma frequency, n_e is the background plasma density, e and m_e are the electron charge and mass, and c is the speed of light. Linear kinetic plasma theory gives estimates of the fastest growth rates of CFI and OBI in the cold distribution function limit [28] as $\Gamma_{CFI} \sim \beta_b\sqrt{\alpha/\gamma_b}\,\omega_p$ and $\Gamma_{OBI} \sim \sqrt{3}/2^{4/3}\,(\alpha/\gamma_b)^{1/3}\,\omega_p$, where β_b and γ_b are the Lorentz factors of the beam and α is the beam-plasma density ratio. Together, these set a requirement that the density of the e^+e^- pair beams must be sufficiently large that collective plasma instabilities grow fast enough to be observed on laboratory timescales, while the background plasma is dense enough for the skin depth to be smaller than the physical beam size. A proposed plasma generation that satisfies these requirements will be discussed in detail in Sec. V.

The easiest way to produce a high density of electron-positron pairs from a high-energy photon beam is the conversion process in a high-Z material, such as lead. In a scheme which uses GeV/c protons, preliminary Monte Carlo simulations indicate that we can increase the maximum pair beam density above what can be obtained by a lead converter alone. We do this by preceding the converter with a beryllium target. Beryllium has a relatively short nucleon interaction length compared with its radiation length, such that a large number of high-energy γ can be generated from π^0 decays in the beryllium with minimal subsequent scattering. This additional flux of photons enhances the densities of pairs that can be generated in the lead converter. A schematic demonstrating this idea is shown in Fig. 1.

III. MONTE CARLO SIMULATIONS

To better understand the pair beams created by this scheme, Monte Carlo modeling was performed using the particle transport code FLUKA [29,30], which can accurately simulate hadronic interactions and electromagnetic cascades as a 400 GeV/c proton beam propagates through a solid target

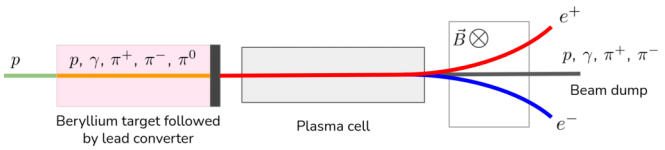

FIG. 1. Proposed experimental setup. Beams composed of electrons, positrons, photons, protons, and other hadrons are generated using a beryllium target followed by a lead converter. The beam-plasma interaction can be studied by driving the beam into a plasma cell. For this plasma cell, an inductively coupled discharge is proposed in Sec. V. Since the bulk of the electrons and positrons in the beam have much smaller momentum than the hadrons, dipole magnets can be used to deflect e^+e^- out of the beam to study their energy spectra, while the hadrons are deflected less and are absorbed by the beam dump.

of beryllium and lead. As an input for the simulations, we assume a proton beam corresponding to repeatable experimental conditions at HiRadMat, i.e., a collimated proton beam with an essentially monochromatic spectral profile peaked at 440 GeV/c (with width corresponding to 0.03% from the central energy) and a Gaussian transverse beam profile with $\sigma = 0.5$ mm. To obtain reasonable statistics, more than 10^5 protons were simulated to interact with various combinations of thicknesses of beryllium target and lead converter. Beam characteristics such as size, divergence, and energy spectra were recorded for the different components of the generated beams escaping the converter rear.

The results show that for primary beams containing 10^{11} protons, generated beams contain a dominating fluence of 10^{13}–10^{14} electron-positron pairs and γ rays, along with a smaller number (several tens of times smaller) of protons and other hadron species, the most numerous of these being charged pions.

The transverse radial beam profiles of different beam components are reasonably well described by a Lorentzian function, and fitting was used to obtain FWHM beam diameters and peak fluences. Estimates of peak volume densities were obtained from peak fluences by assuming the length of the generated beams to be approximately 11.4 cm in the HiRadMat setup. This length corresponds to a beam duration of 375 ps and accounts for the effect of particle straggling in the target, which simulations show to be $\lesssim$5 ps.

The dependencies of peak component densities on target and converter thicknesses can be found in Fig. 2 for four cases; Figs. 2(a) and 2(b) show the peak particle densities when beryllium and lead are used on their own, while Figs. 2(c) and 2(d) show the sensitivities of particle densities to a change in thickness of beryllium or lead from a configuration which gives a high density of e^+e^- pairs (30-cm beryllium target and 4-cm lead converter). As expected, we immediately see that e^+e^- density is much more sensitive to the thickness of the high-Z lead converter. An increase in target thickness will only increase the density of a beam component if additional particle generation is more significant than density decreases due to beam divergence or depletion of particles in processes such as decay, absorption, and annihilation. In all four plots, proton density decreases with target thickness, as protons scatter off the target nuclei. This is more noticeable in the

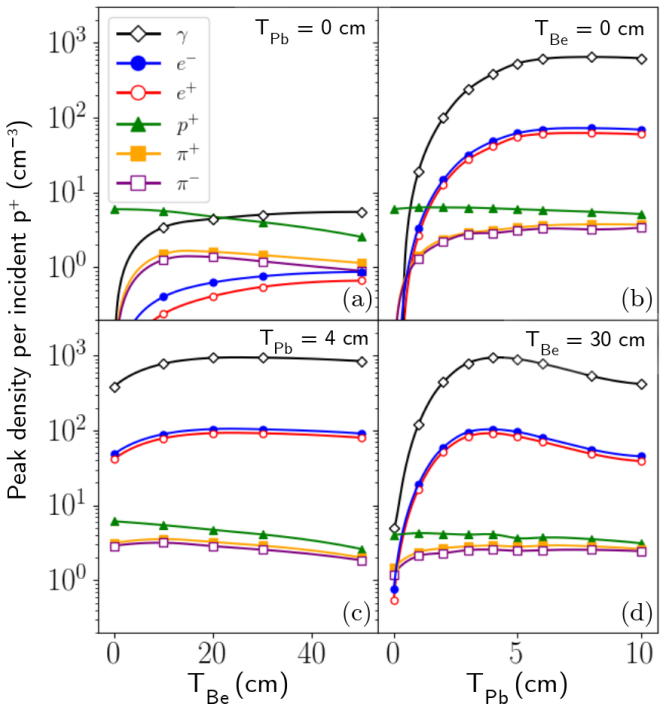

FIG. 2. The dependencies of peak densities of each beam species on Be target and Pb converter thicknesses is shown for four configurations. (a) and (b) show the densities obtained for single-component targets of beryllium and lead, while (c) and (d) show the sensitivities of particle densities to a change in thickness of beryllium or lead from a configuration that generates a high density of e^+e^- pairs (that is, 30-cm beryllium target with a 4-cm lead converter). The largest pair beam densities are only achieved by using a configuration that contains both beryllium and lead, and the thickness of lead can be modified to alter the ratio of e^+e^- to hadrons in the beam. Densities are obtained assuming an incident p^+ beam with radius $\sigma = 0.5$ mm and are presented in units per incident proton, so that the numbers can be scaled to the bunch intensity of the proton facility. A pulse duration of 375 ps is assumed to obtain the peak density from the simulated peak fluence.

beryllium thickness scans, which cover more nuclear collision lengths than the lead scans. The density of electron-positron pairs increases as soon as high-energy photons are generated and cascades are initiated, but densities of photons and e^+e^- pairs are higher in lead, where the length scale associated with initiation of electromagnetic cascades is much smaller.

By comparing the peak densities of pairs in these four plots, we can see that the largest pair beam densities and the largest ratios of pair density to hadron density can only be achieved by using a configuration that contains both beryllium and lead. Using a 30-cm beryllium target and 4-cm lead converter can lead to e^+e^- pair densities in excess of 10^{13} cm^{-3} (see column 3 of Table II). Higher densities are achievable with higher-intensity proton pulses of smaller beam diameter. The thickness of lead can be modified in an experiment to dramatically adjust the ratio of densities of e^+e^- to hadrons, without changing the hadron density significantly. This can allow us to probe jets with a variety of compositions.

For the case of a 30-cm beryllium target and 4-cm lead converter, Fig. 3 shows the energy spectra and angle-position

TABLE II. Summary of the characteristics of significant particle components of the generated beam, obtained from Monte Carlo numerical simulations for the case of a beryllium target and lead converter with thicknesses of 30 and 4 cm, respectively. All quantities are calculated based on the particles which escape the rear surface of the lead converter. The peak fluence and beam diameter are obtained by fitting the transverse density profile of the escaping beam to a Lorentzian profile. Similarly the beam divergence is the FWHM of the angular distribution of the escaping beam fitted to a Lorentzian profile. The peak fluence is used to infer the peak volume density in the laboratory frame by assuming the generated beam has a length of 11.4 cm. Yield and peak densities are given per 10^{11} incident protons with a beam radius $\sigma = 0.5$ mm.

Species	Yield per 10^{11} p^+	Peak density per 10^{11} p^+ (cm^{-3})	Divergence (mrad)	Beam diameter (mm)
e^-	1.5×10^{13}	1.0×10^{13}	25.3	2.6
e^+	1.3×10^{13}	0.9×10^{13}	25.3	2.6
p^+	4.0×10^{11}	4.1×10^{11}	0.28	1.3
π^+	5.5×10^{11}	2.9×10^{11}	10.0	1.9
π^-	5.6×10^{11}	2.6×10^{11}	11.9	2.0
γ	2.8×10^{14}	9.4×10^{13}	17.0	3.0

phase space plots for the significant beam components as they emerge from the rear of the converter.

The e^+ and e^- spectra are very similar, differing only at energies less than 10 MeV, where the annihilation cross section of positrons becomes significant. The spectra are dominated by particles which have only tens of MeV, but extend up to tens of GeV in their high-energy tails. These characteristics are matched by the photon spectra, with the addition of a spectral peak at 511 keV resulting from electron-positron annihilation.

The proton spectra appear bimodal in distribution. We see a peak at 440 GeV corresponding to the protons in the initial beam which have not lost a significant fraction of their energy, and we also see much lower energy protons resulting from the inelastic hadronic scattering. Spectra with similar characteristics are seen for the charged pions, except with the omission of the high-energy contribution from an initial beam.

We can get an idea of the extent to which high beam densities are maintained as the beam propagates by looking at its overall divergence (the distribution of the angles between the beam axis and the particle trajectory of all the particles of a species as they exit the rear of the converter). For e^+e^- and γ we observe that the emerging beams have an overall divergence of 15–30 mrad (see column 4 of Table II). The pions have a divergence of 10 mrad, which means the ratio of beam density of pions to e^+e^- will not change much as the beam propagates. The lower divergence of the protons due to the directionality of the high-energy component of the beam means that care must be taken to position the plasma cell close to the converter rear in order to maximize the dominance of e^+e^- pair density over proton density.

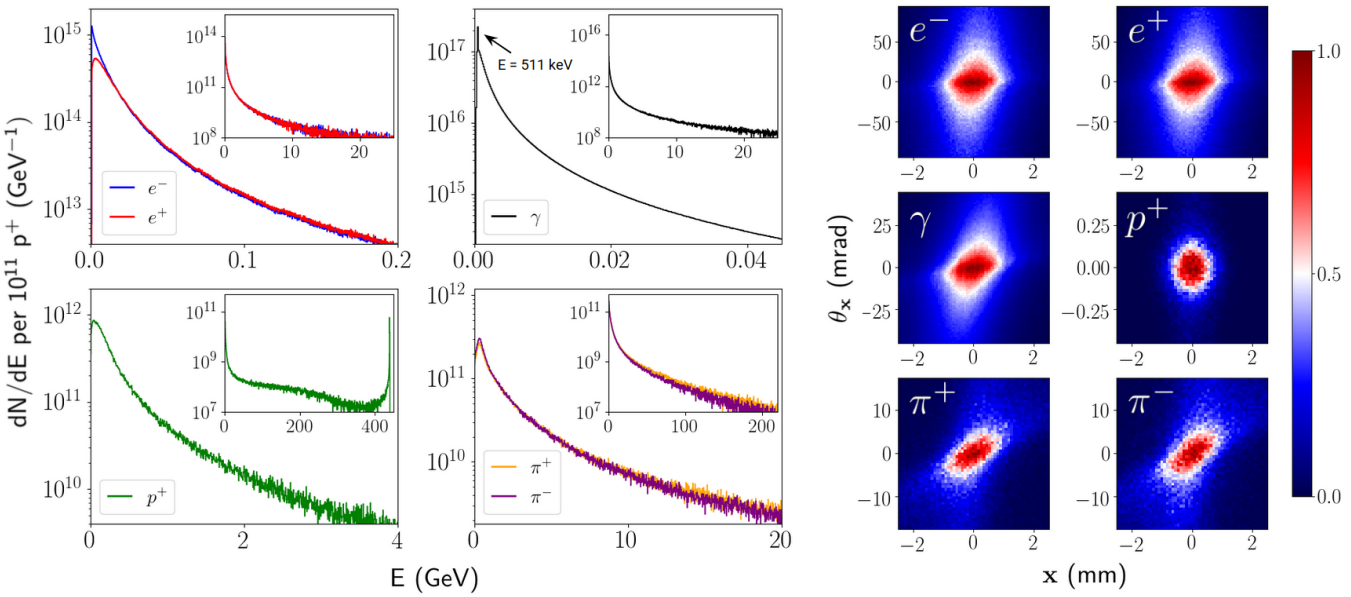

FIG. 3. Energy spectra (left) and angle-position phase space plots (right) obtained in the case of a 30-cm beryllium target and 4-cm lead converter. The simulation setup is the same as the one mentioned in Table II. The energy spectra are displayed in the ranges where their spectra are most significant, while insets display the spectra extending to much higher energies. In the angle-position phase space plots, **x** refers to the position along the in-plane transverse direction, and z is the longitudinal direction. $\theta_{\mathbf{x}}$ is the angle $\arctan(v_x/v_z)$, where v_x and v_z are the components of the particle velocity along the x and z axes (measured in the laboratory frame). The plots are normalized and displayed with a color mapping that clearly depicts the half maxima.

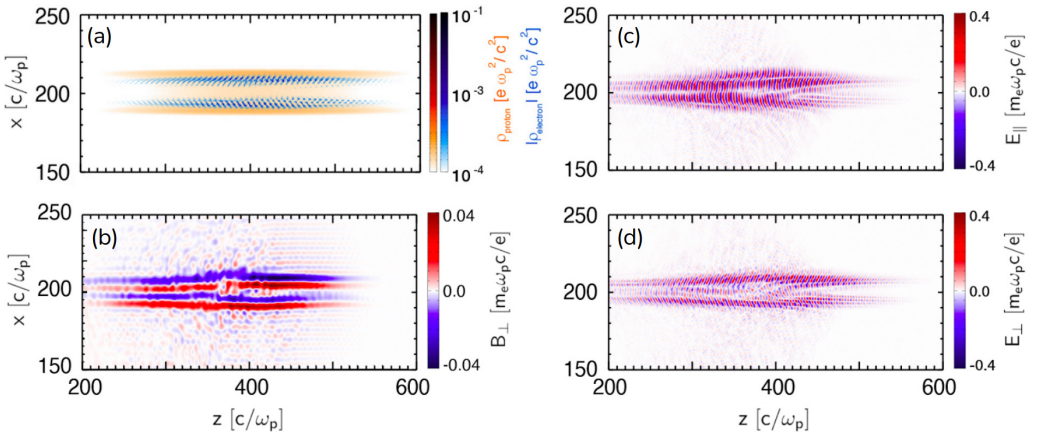

FIG. 4. Simulation results of the interaction between an electron-positron-proton bunch and a static plasma with density 10^{14} cm^{-3} at a time $t = 705\ [1/\omega_p] = 1.27$ ns. (a) Density filaments of electrons (blue) and protons (orange). (b) Transverse magnetic field $B_\perp$ filaments due to current filamentation. (c) Longitudinal electric fields $E_\parallel$ and (d) transverse electric fields $E_\perp$ attributed to charge separation and inductive effects. Units are such that one plasma period $[1/\omega_p]$ corresponds to $[1/\omega_p] = 1.8$ ps, while one skin depth $[c/\omega_p]$ corresponds to $[c/\omega_p] = 530\ \mu$m, and magnetic and electric field units are $[m_e\omega_p c/e] = 3.2$ T and $[m_e\omega_p c/e] =$ GV/m, respectively.

For all beam components we find the initial beam diameter to be millimeter scale (see column 5 of Table II). Choosing e^+e^- beam mean Lorentz factors $\gamma_b \sim 100$, and background plasma densities that lead to a larger transverse beam size than the background plasma skin depth, analytical growth rates for CFI and OBI are closely competing and on the order of picoseconds. However, for beams such as ours, which are relativistically hot ($k_B T > m_e c^2$), the true scalings and growth rates will be different from the cold beam approximations. We have performed PIC simulations to better understand the nonlinear growth of CFI and OBI in the case of our $e^-e^+p^+$ beams propagating through a background plasma. From PIC simulations we can gain better insight into the competition between CFI and OBI growth, and better estimates of the timescales for instability growth and saturation. We can also obtain the magnitude of the energy expected to be converted into magnetic and electric fields, and whether the generated fields are of a sufficiently high magnitude that they might be measurable in an experiment.

IV. PARTICLE-IN-CELL SIMULATIONS

The fully relativistic, massively parallel, PIC code OSIRIS [31,32], which has been used extensively to model relativistic beam-plasma interactions [33–35], was used to perform PIC simulations of an electron-positron-proton bunch through a background plasma. The platform we present generates beams with dramatically increased duration compared with quasineutral e^+e^- beams generated at laser facilities (which are limited to having beam durations of tens to hundreds of femtoseconds) [20–24]. The computational cost of simulating beams of 400-ps duration for long propagation times (up to several nanoseconds) prevents us from performing full three-dimensional (3D) PIC simulations. However, in simulations of beams with shorter duration and propagation distances, for which 3D simulations are possible, 2D simulations have been shown to offer a good approximation [34]. In particular, the linear growth rate of the instability is shown to be the same in 2D and 3D, and equivalent filamentation structures develop. It is expected that 2D simulations might underestimate the saturated magnetic field strength, but they will nevertheless offer useful insight into the underpinning physics.

The simulations used a moving window traveling at c, with absorbing boundary conditions, and dimensions $800 \times 400\ (c/\omega_p)^2$ divided into 8000×4000 cells with 6×6 particles per cell for plasma electrons and beam particles. Electron-positron-proton beams were initialized at the entrance of a stationary plasma with density profile given by $n_b = n_{b0} \exp(-r^2/\sigma_r^2 - z^2/\sigma_z^2)$, where the bunch peak densities are $n_{b0} = 10^{13}$ cm^{-3} for electrons and positrons and $n_{b0} \sim 10^{11}$ cm^{-3} for the protons. The bunch length and transverse waist are $\sigma_z = 7.0$ cm $= 132\ c/\omega_p$ and $\sigma_r = 0.15$ cm $= 2.8\ c/\omega_p$, respectively, with the skin depth of the background plasma c/ω_p corresponding to a plasma density $n_p = 10^{14}$ cm^{-3}. An ion-electron mass ratio $m_p/m_e = 1836$ is used.

Studies which have investigated the effect of temperature on growth of filamentation and oblique modes have found that growth rates are strongly suppressed in beams with large transverse temperature [36] but are less dependent on large longitudinal energy spreads [34]. Therefore we set each beam component to propagate along the z axis with Lorentz factor set by the mean longitudinal momentum (without a thermal momentum spread), while a thermal momentum spread is included in the transverse direction that corresponds to the mean transverse momentum. For the electrons and positrons, we choose a bulk Lorentz factor of $\gamma \sim \langle p_\parallel \rangle / m_e c \sim 100$ and transverse thermal spread of 7.5 MeV. For the protons, $\gamma \sim \langle p_\parallel \rangle / m_p c \sim 50$ with transverse thermal spread 370 MeV. The divergence of the e^+e^- beam is initialized as 52 mrad (FWHM) and then evolves self-consistently.

Simulation results are illustrated in Fig. 4, showing the spatial-temporal evolution of protons and electrons in the beam [Fig. 4(a)], the formation of transverse magnetic filaments [Fig. 4(b)], and the typical electric field structure [Figs. 4(c) and 4(d)]. In our simulations we observe the breaking up of the beam into current filaments (with width on

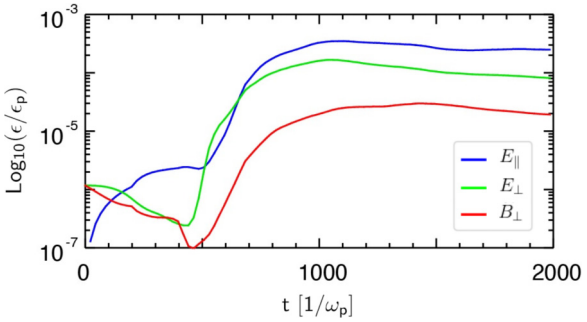

FIG. 5. Evolution of energies contained within transverse magnetic field $\epsilon_{B\perp}$ (red, lower curve), transverse electric field $\epsilon_{E\perp}$ (green, middle curve), and longitudinal electric field $\epsilon_{E\parallel}$ (blue, upper curve) as the beam propagates, normalized to the initial kinetic energy of the beam $\epsilon_\mathrm{p} = 2n_\mathrm{b}Vm_\mathrm{e}c^2(\gamma_\mathrm{b} - 1)$, where V is the volume of the beam and $2n_\mathrm{b}$ is the combined density of the e^- and e^+ in the beam.

the order of $c/\omega_\mathrm{p} \sim 500\ \mu$m) as the electron-positron-proton bunch enters into the background plasma. Any charge separation in the beam generates microcurrents, which reinforces initial perturbations, causing the growth of electromagnetic plasma instability and the exponential growth of electromagnetic fields. This is demonstrated in Fig. 5, where the temporal evolution of the magnetic and electric field energies is shown as a function of time, normalized to the initial bulk kinetic energy of the beam.

The fields saturate after $t = 1000\ [1/\omega_\mathrm{p}] = 1.8$ ns, and magnetic fields with amplitudes of 0.13 T are generated via the current filamentation instability (corresponding to $\sim 10^{-5}$ of the initial beam energy). Simultaneously, longitudinal and transverse electric fields are observed with magnitudes exceeding 300 MV/m, which can be attributed to space charge and inductive effects [34].

Our simulations show the emergence of oblique modes and tilted filamentation, which reduces the growth of magnetic fields. This behavior is observed in previous simulation studies [34]. Importantly, in order for OBI to compete with CFI, such that the growth of oblique modes has an effect on magnetic field generation, the beam length must be sufficiently long to allow coupling between the transverse and longitudinal instability modes. This is the case for the beams generated in this platform, which have longitudinal length that extends over many plasma wavelengths of the background plasma.

V. INDUCTIVELY COUPLED PLASMA DISCHARGE

To create a plasma with sufficiently large volume and electron density to study the growth of beam-plasma instabilities, we consider using a cylindrical inductively coupled plasma (ICP) discharge [37,38]. In its simplest form, this consists of a tube made of a dielectric material placed inside a solenoid coil through which a radio-frequency current is applied. When a large enough current is applied to the coil, a gas discharge can be sustained by azimuthal electric fields that are induced by the time-varying magnetic field. In this mode of operation, the system can be modeled as a transformer with the inductive coil taken as the primary circuit and the plasma as the secondary circuit [39].

Given that we expect the transverse size of the electron-positron-hadron beams to grow from millimeter scale to centimeter scale after a few tens of centimeters of propagation, we can lower the required background plasma density to 10^{11}–10^{12} cm^{-3} and still ensure that the length scale of current filaments remains smaller than the transverse beam size. Since the analytical growth rates of CFI and OBI scale with $\sqrt{n_\mathrm{e}}$, this does not result in an excessive slowdown of instability growth, but it does bring the required background plasma density within realistic operating parameters of an inductive discharge source.

Successful analytical models have been devised to predict the plasma parameters for a low-pressure discharge such as the ICP discharge, for given tube geometry, gas pressure, and applied electrical parameters [38,40,41]. The simplest of these models, the volume-averaged global model, assumes a uniform density profile $n = n_0$ throughout the discharge except near the wall, where the electron density drops sharply to a sheath-edge density n_s, with the sheath thickness not expected to exceed more than a few plasma Debye lengths. Then, steady-state, volume-averaged electron temperature and density can be estimated by particle and power balance. Argon is commonly chosen as a discharge gas, and it is simple to treat analytically. We follow the typical assumption in these models of Maxwellian electron energy distribution.

Electron temperature can be determined by equating the volume ionization to the surface particle loss. For a tube with radius R, length L, and neutral gas density n_g,

$$K_\mathrm{iz} n_\mathrm{g} n_0 (\pi R^2 L) = n_0 u_\mathrm{B} (2\pi R^2 h_L + 2\pi R L h_R), \tag{1}$$

where K_iz is the rate of electron-neutral ionization, $u_\mathrm{B} = \sqrt{k_\mathrm{B} T_\mathrm{e}/m_\mathrm{i}} \approx 9.81 \times 10^3\ (T_\mathrm{e}\ [\mathrm{eV}]/A)^{1/2}$ ms^{-1} is the Bohm (ion loss) velocity, m_i is the ion mass, and A is the atomic mass number. Sheath-edge density n_s is related to bulk plasma density n_0 via [38,42]

$$h_L = \frac{n_{s_L}}{n_0} \approx 0.86\left(3 + \frac{L}{2\lambda_\mathrm{i}}\right)^{-1/2} \tag{2}$$

at the axial sheath edge and

$$h_R = \frac{n_{s_R}}{n_0} \approx 0.80\left(4 + \frac{R}{\lambda_\mathrm{i}}\right)^{-1/2} \tag{3}$$

at the radial sheath edge; λ_i is the ion-neutral mean free path $\lambda_\mathrm{i} = 1/n_\mathrm{g}\sigma_\mathrm{i} \approx 3.03(p\ [\mathrm{mTorr}])^{-1}$ cm, under the assumption that the total ion-atom scattering cross section for low-energy ions ($T_i \approx 0.05$ eV) is approximately $\sigma_\mathrm{i} \approx 10^{-14}$ cm^2 [38]. These expressions for h_R and h_L apply in the regime that $(R, L) \gtrsim \lambda_\mathrm{i} \gtrsim (T_\mathrm{i}/T_\mathrm{e})(R, L)$, which holds if we choose $n_\mathrm{g} \sim 10^{14}$–$10^{15}$ cm^{-3} (pressures between 3 and 30 mTorr at room temperature) for a chamber with $R \sim 2.5$ cm and $L \sim 0.5$–1 m.

To estimate T_e, we need the rate coefficient for electron-neutral ionization, which is obtained from measurements [43]. A fit applicable to the range $1 \leqslant T_\mathrm{e} \leqslant 7$ eV yields $K_\mathrm{iz} \approx 2.34 \times 10^{-14}\, T_\mathrm{e}^{0.59} \exp(-17.44/T_\mathrm{e})$ m^3/s, with T_e in eV [44].

Electron density can be determined by equating the power absorbed by the plasma to the power lost due to all electron-neutral collision processes in the volume, and ion and electron

TABLE III. Plasma parameters for argon plasma, $R = 2.5$ cm and $L = 1$ m.

n_g (cm^{-3})	p (mTorr)	T_e (eV)	$\mathcal{E}_T$ (V)	n_0 (cm^{-3})
10^{14}	3	4.2	72.4	5.4×10^{11}
10^{15}	30	2.4	100.6	1.1×10^{12}

energy loss to the walls. That is,

$$P_{abs} = en_0 u_B \mathcal{E}_T (2\pi R^2 h_L + 2\pi R L h_R), \quad (4)$$

where P_{abs} is the power delivered to the plasma through the inductive coupling and $\mathcal{E}_T = \mathcal{E}_c + \mathcal{E}_e + \mathcal{E}_i$ is the sum of the collisional energy lost per electron-ion pair created and the kinetic energy lost per electron or ion lost from the system. Expressions for $\mathcal{E}_T$ can be derived and are generally a function of T_e and the cross sections for collisions and excitation of the gas and plasma species [38,44]. Table III shows values for T_e, $\mathcal{E}_T$, and n_0 calculated for a discharge using this model, with $R \sim 2.5$ cm, $L \sim 1$ m, typical driving frequency $f = 13.56$ MHz, $n_g \sim 10^{14}$–10^{15} cm^{-3}, and $P_{abs} = 1000$ W, assuming the gas temperature to be room temperature. The electron density n_0 scales linearly with P_{abs}. P_{abs} can differ from the power supplied by the rf source but is expected to be several hundreds of watts for a kilowatt power source with a good impedance matching.

Figure 6 shows an example design for an inductive discharge that can be used in experiments such as this which require large-volume plasmas with electron densities exceeding 10^{11} cm^{-3}. Coils wrapped around sections of glass tube are connected to an rf power source via an impedance matching network. Port crosses can be included in the design to insert diagnostics, with the coils arranged so that the generated plasma extends between the coils. Before the experiment, the plasma parameters can be fully characterized for the specific design using a Langmuir probe.

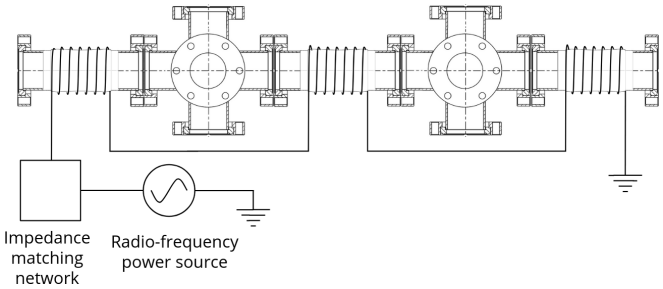

FIG. 6. The design for a cylindrical inductive discharge composed of coils wrapped around sections of glass tube. The glass tubes are separated by port crosses where diagnostics can be inserted. The coils are connected to a radiofrequency power source via an impedance matching network that ensures maximum coupling of electrical power into the plasma. The generated plasma is expected to extend between the coils, which means they can be spaced apart.

VI. SUMMARY

The growth of kinetic plasma instabilities of relevance to astrophysical phenomena such as GRBs has been investigated for an experimental platform in which low-divergence, ultradense, quasineutral, electron-positron pair beams are generated using 400 GeV/c protons available at facilities such as AWAKE and HiRadMat at CERN.

Monte Carlo simulations demonstrate the possibility of generating beams that contain 10^{13}–10^{14} electron-positron pairs along with a smaller number (10^{11}–10^{12}) of hadrons such as protons and pions. Particle-in-cell simulations have shown that beams interacting with a background plasma will exhibit collective plasma effects and the generation of magnetic fields exceeding 0.1 T via filamentation instabilities, which saturate after 50 cm of beam propagation.

This platform represents a significant step forward for experiments aimed at exploring relativistic pair-plasma phenomena in a laboratory setting. We have demonstrated the experimental feasibility of isolating and studying the nonlinear evolution of several key instabilities that are presently limited to numerical experiments, allowing for the possibility of observing the effects of obliquely growing filamentation modes and the role of hadrons on magnetic field generation in the development of kinetic plasma instabilities. By changing experimental parameters such as incident proton density, target thickness, and density of background plasma, different configurations corresponding to fireballs traversing an overdense or underdense background medium can be examined, and the composition of different astrophysical scenarios can be studied.

ACKNOWLEDGMENTS

The research leading to these results has received funding from AWE plc., the Central Laser Facility (Science and Technology Facilities Council of the United Kingdom), the European Research Council (through Grant No. ERC-2015-AdG, Grant Agreement No. 695088), Fundação para a Ciência e Tecnologia (through Grant No. EXPL/FIS-PLA/0834/2012), and the Department of Energy Office of Fusion Energy (Grant No. DE-SC0017950). R.B. acknowledges support from EPSRC grant EP/R004773/1. The work of G.G. was partially supported by EPSRC Grant No. EP/M022331/1 and EP/N014472/1. FLUKA simulations were performed using the Science and Technology Facilities Council Scientific Computing Department's SCARF cluster, and OSIRIS simulations were performed at the Marconi-Broadwell (CINECA, Italy).

This paper was written by C.D.A. with contributions from N.S., N.C., J.T.G., B.R., S.S., R.B. and G.G. FLUKA simulations were performed by C.D.A., and N.S. performed OSIRIS simulations. N.C., Y.K., B.T.H. and T.D. contributed to the definition of the experimental setup, while R.B., H.C., D.H.F., S.R., J.L.S., L.O.S., and R.M.G.M.T. provided theoretical and diagnostics support. This project was conceived by R.B. and G.G.

[1] P. Goldreich and W. H. Julian, Pulsar electrodynamics, Astrophys. J. **157**, 869 (1969).

[2] J. Arons, Pair creation above pulsar polar caps–Geometrical structure and energetics of slot gaps, Astrophys. J. **266**, 215 (1983).

[3] R. D. Blandford and R. L. Znajek, Electromagnetic extraction of energy from Kerr black holes, Mon. Not. R. Astron. Soc. **179**, 433 (1977).

[4] M. C. Begelman, R. D. Blandford, and M. J. Rees, Theory of extragalactic radio sources, Rev. Mod. Phys. **56**, 255 (1984).

[5] *Active Galactic Nuclei: Proceedings of a Conference Held at the Georgia State University, Atlanta, Georgia, October 28–30, 1987*, edited by H. R. Miller and P. J. Wiita, Lecture Notes in Physics Vol. 307 (Springer, New York, 1988).

[6] J. Wardle, D. Homan, R. Ojha, and D. Roberts, Electron–positron jets associated with the quasar 3C279, Nature (London) **395**, 457 (1998).

[7] P. Meszaros and M. Rees, Relativistic fireballs and their impact on external matter: Models for cosmological gamma-ray bursts, Astrophys. J. **405**, 278 (1993).

[8] T. Piran, The physics of gamma-ray bursts, Rev. Mod. Phys. **76**, 1143 (2005).

[9] A. Gruzinov, Gamma-ray burst phenomenology, shock dynamo, and the first magnetic fields, Astrophys. J., Lett. **563**, L15 (2001).

[10] P. Chang, A. Spitkovsky, and J. Arons, Long-term evolution of magnetic turbulence in relativistic collisionless shocks: electron-positron plasmas, Astrophys. J. **674**, 378 (2008).

[11] S. Bludman, K. Watson, and M. Rosenbluth, Statistical mechanics of relativistic streams. II, Phys. Fluids **3**, 747 (1960).

[12] R. Lee and M. Lampe, Electromagnetic Instabilities, Filamentation, and Focusing of Relativistic Electron Beams, Phys. Rev. Lett. **31**, 1390 (1973).

[13] B. B. Godfrey, W. R. Shanahan, and L. E. Thode, Linear theory of a cold relativistic beam propagating along an external magnetic field, Phys. Fluids **18**, 346 (1975).

[14] M. V. Medvedev and A. Loeb, Generation of magnetic fields in the relativistic shock of gamma-ray burst sources, Astrophys. J. **526**, 697 (1999).

[15] A. Bret, Weibel, two-stream, filamentation, oblique, Bell, Buneman...which one grows faster? Astrophys. J. **699**, 990 (2009).

[16] J.-I. Sakai, R. Schlickeiser, and P. K. Shukla, Simulation studies of the magnetic field generation in cosmological plasmas, Phys. Lett. A **330**, 384 (2004).

[17] M. V. Medvedev and A. Spitkovsky, Radiative cooling in relativistic collisionless shocks: Can simulations and experiments probe relevant gamma-ray burst physics? Astrophys. J. **700**, 956 (2009).

[18] I. Efthymiopoulos, C. Hessler, H. Gaillard, D. Grenier, M. Meddahi, P. Trilhe, A. Pardons, C. Theis, N. Charitonidis, S. Evrard, H. Vincke, and M. Lazzaroni, HiRadMat: A New Irradiation Facility for Material Testing at CERN, Technical Report CERN-ATS-2011-232, CERN (2011).

[19] E. Gschwendtner, E. Adli, L. Amorim, R. Apsimon, R. Assmann, A.-M. Bachmann, F. Batsch, J. Bauche, V. B. Olsen, M. Bernardini, R. Bingham, B. Biskup, T. Bohl, C. Bracco, P. N. Burrows, G. Burt, B. Buttenschön, A. Butterworth, A. Caldwell, M. Cascella *et al.*, AWAKE, the advanced proton driven plasma Wakefield acceleration experiment at CERN, Nucl. Instrum. Methods Phys. Res., Sect. A **829**, 76 (2016).

[20] G. Sarri, K. Poder, J. Cole, W. Schumaker, A. Di Piazza, B. Reville, T. Dzelzainis, D. Doria, L. Gizzi, G. Grittani, S. Kar, C. H. Keitel, K. Krushelnick, S. Kuschel, S. P. D. Mangles, Z. Najmudin, N. Shukla, L. O. Silva, D. Symes, A. G. R. Thomas *et al.*, Generation of neutral and high-density electron–positron pair plasmas in the laboratory, Nat. Commun. **6**, 6747 (2015).

[21] G. J. Williams, B. B. Pollock, F. Albert, J. Park, and H. Chen, Positron generation using laser-Wakefield electron sources, Phys. Plasmas **22**, 093115 (2015).

[22] T. Xu, B. Shen, J. Xu, S. Li, Y. Yu, J. Li, X. Lu, C. Wang, X. Wang, X. Liang, Y. Leng, R. Li, and Z. Xu, Ultrashort megaelectronvolt positron beam generation based on laser-accelerated electrons, Phys. Plasmas **23**, 033109 (2016).

[23] J. Warwick, T. Dzelzainis, M. E. Dieckmann, W. Schumaker, D. Doria, L. Romagnani, K. Poder, J. M. Cole, A. Alejo, M. Yeung, K. Krushelnick, S. P. D. Mangles, Z. Najmudin, B. Reville, G. M. Samarin, D. D. Symes, A. G. R. Thomas, M. Borghesi, and G. Sarri, Experimental Observation of a Current-Driven Instability in a Neutral Electron-Positron Beam, Phys. Rev. Lett. **119**, 185002 (2017).

[24] G. J. Williams, H. Chen, J. Kim, S. Kerr, and H. Y. Khater, Comment on "Table-top Laser-Based Source of Femtosecond, Collimated, Ultrarelativistic Positron Beams", Phys. Rev. Lett. **124**, 179501 (2020).

[25] K. Asano, S. Guiriec, and P. Meszaros, Hadronic models for the extra spectral component in the short GRB 090510, Astrophys. J., Lett. **705**, L191 (2009).

[26] K. Asano, S. Inoue, and P. Mészáros, Prompt high-energy emission from proton-dominated gamma-ray bursts, Astrophys. J. **699**, 953 (2009).

[27] N. Shukla, A. Stockem, F. Fiúza, and L. O. Silva, Enhancement in the electromagnetic beam-plasma instability due to ion streaming, J. Plasma Phys. **78**, 181 (2012).

[28] A. Bret and C. Deutsch, Stabilization of the filamentation instability and the anisotropy of the background plasma, Phys. Plasmas **13**, 022110 (2006).

[29] A. Ferrari, P. R. Sala, A. Fasso, and J. Ranft, FLUKA: A Multi-particle Transport Code, Technical Report SLAC-R-773, Stanford Linear Accelerator Center (2005).

[30] T. Böhlen, F. Cerutti, M. Chin, A. Fassò, A. Ferrari, P. G. Ortega, A. Mairani, P. R. Sala, G. Smirnov, and V. Vlachoudis, The FLUKA code: Developments and challenges for high energy and medical applications, Nucl. Data Sheets **120**, 211 (2014).

[31] R. A. Fonseca, L. O. Silva, F. S. Tsung, V. K. Decyk, W. Lu, C. Ren, W. B. Mori, S. Deng, S. Lee, T. Katsouleas, and J. C. Adam, OSIRIS: A three-dimensional, fully relativistic particle in cell code for modeling plasma based accelerators, in *International Conference on Computational Science*, Lecture Notes in Computer Science Vol. 2331 (Springer, New York, 2002), pp. 342–351.

[32] R. A. Fonseca, S. F. Martins, L. O. Silva, J. W. Tonge, F. S. Tsung, and W. B. Mori, One-to-one direct modeling of experiments and astrophysical scenarios: Pushing the envelope on kinetic plasma simulations, Plasma Phys. Controlled Fusion **50**, 124034 (2008).

[33] L. O. Silva, R. A. Fonseca, J. W. Tonge, J. M. Dawson, W. B. Mori, and M. V. Medvedev, Interpenetrating plasma shells: Near-equipartition magnetic field generation and non-thermal particle acceleration, Astrophys. J., Lett. **596**, L121 (2003).

[34] N. Shukla, J. Vieira, P. Muggli, G. Sarri, R. Fonseca, and L. O. Silva, Conditions for the onset of the current filamentation instability in the laboratory, J. Plasma Phys. **84**, 905840302 (2018).

[35] N. Shukla, S. F. Martins, P. Muggli, J. Vieira, and L. O. Silva, Interaction of ultra relativistic e^-e^+ fireball beam with plasma, New J. Phys. **22**, 013030 (2020).

[36] A. Bret, L. Gremillet, and M. E. Dieckmann, Multidimensional electron beam-plasma instabilities in the relativistic regime, Phys. Plasmas **17**, 120501 (2010).

[37] J. J. Thomson, The electrodeless discharge through gases, Philos. Mag. 7 **4**, 1128 (1927).

[38] M. A. Lieberman and A. J. Lichtenberg, *Principles of Plasma Discharges and Materials Processing*, 2nd ed. (John Wiley, New York, 2005).

[39] J. J. Thomson, On the discharge of electricity through exhausted tubes without electrodes, Philos. Mag. **32**, 445 (1891).

[40] M. A. Lieberman and R. A. Gottscho, Design of high-density plasma sources for materials processing, in *Plasma Sources for Thin Film Deposition and Etching*, edited by M. Francombe and J. Vossen, Physics of Thin Films Vol. 18 (Academic, New York, 1994), pp. 1–119.

[41] J. T. Gudmundsson and M. A. Lieberman, Magnetic induction and plasma impedance in a cylindrical inductive discharge, Plasma Sources Sci. Technol. **6**, 540 (1997).

[42] V. A. Godyak, *Soviet Radio Frequency Discharge Research* (Delphic, Falls Church, VA, 1986).

[43] H. C. Straub, P. Renault, B. G. Lindsay, K. A. Smith, and R. F. Stebbings, Absolute partial and total cross sections for electron-impact ionization of argon from threshold to 1000 eV, Phys. Rev. A **52**, 1115 (1995).

[44] J. T. Gudmundsson and M. A. Lieberman, Technical Report, Technical Report No. RH-21-2002, Science Institute, University of Iceland (2002).